

# Universality in Efimov associated tetramers in $^4\text{He}$

E. Hiyama\*

RIKEN Nishina Center, RIKEN, Wako 351-0198, Japan

M. Kamimura†

Department of Physics, Kyushu University, Fukuoka 812-8581, Japan,  
RIKEN Nishina Center, RIKEN, Wako 351-0198, Japan

(Dated: December 7, 2024)

We calculated, using seven *realistic*  $^4\text{He}$ - $^4\text{He}$  potentials in the literature, the Efimov spectra of  $^4\text{He}$  trimer and tetramer and analyzed the universality of the systems. The three-(four-)body Schrödinger equations were solved fully nonadiabatically with the high-precision calculation method employed in our previous work on the  $^4\text{He}$  trimer and tetramer [Phys. Rev. A **85**, 022502 (2012); **85**, 062505 (2012)]. We found the following universality in the four-boson system: i) The critical scattering lengths at which the tetramer ground and excited states couple to the four-body threshold are independent of the choice of the two-body realistic potentials in spite of the difference in the short-range details and are consistent with the corresponding values observed in the experiments in ultracold alkali atoms when scaled with the van der Waals length  $r_{\text{vdW}}$ , and ii) the four-body hyper-radial potential has a repulsive barrier at the four-body hyperradius  $R_4 \approx 3r_{\text{vdW}}$ , which prevents the four particles from getting close together to explore nonuniversal features of the interactions at short distances. This result is an extension of the universality in Efimov trimers that the appearance of the repulsive barrier at the three-body hyperradius  $R_3 \approx 2r_{\text{vdW}}$  makes the critical scattering lengths independent of the short-range details of the interactions as reported in the literature and also in the present work for the  $^4\text{He}$  trimer with the realistic potentials.

## I. INTRODUCTION

The universal physics of few particles interacting with resonant short-range interactions, commonly referred to as Efimov physics [1], has intensively studied in recent years both experimentally and theoretically (e.g. [2–4] for a review). The resonant short-range two-body interaction with the  $s$ -wave scattering length  $a$  at the unitary limit  $a \rightarrow \pm\infty$  generates the effective three-body attraction that supports an infinite number of weakly bound three-body states, known as the Efimov trimers, with the peculiar geometric universal scaling of their energies. For a potential with a finite scattering length  $a$ , only a finite number of the three-body bound states exist. The critical scattering length,  $a_-^{(0)}$ , for the appearance of the first Efimov state at the three-body threshold on the  $a < 0$  side, often referred to as the three-body parameter, was initially considered as a nonuniversal quantity to be affected by the short-range details of the interactions. The absolute position of  $a_-^{(0)}$ , which determines the overall scale of the whole Efimov spectrum, is not predicted by the low-energy effective theories [1, 3, 4].

However, several recent experiments with identical ultracold alkali atoms suggested that the three-body parameter  $a_-^{(0)}$  might be universal since the observed values in Refs. [5–16] are approximately the same in units of the van der Waals length  $r_{\text{vdW}}$  for different atoms,  $a_-^{(0)}/r_{\text{vdW}} \approx -9.5 \pm 15\%$  as summarized in Refs. [12, 17–

19], where  $r_{\text{vdW}} = \frac{1}{2}(mC_6/\hbar^2)^{1/4}$  with the atomic mass  $m$  and the coefficient  $C_6$  of the long-range potential  $r^{-6}$ .

This interesting result has stimulated the theoretical studies in Refs. [18, 21–25]. In Ref. [18], with a numerical study in the adiabatic hyperspherical representation, the universality of the three-body parameter  $a_-^{(0)}/r_{\text{vdW}}$  has been understood as follows: The origin of the universality is related to the suppression of the probability to find two particles at distances  $r \lesssim r_{\text{vdW}}$  where the pairwise interaction features a deep well supporting many two-body bound states or a short-range hardcore repulsion. This suppression leads to the formation of the universal three-body potential barrier around the three-body hyperradius  $R_3 \approx 2r_{\text{vdW}}$  (see Eq. (2.2) below for the definition of the  $A$ -body hyperradius). This barrier prevents the three particles from simultaneously getting close together to explore nonuniversal features of the interactions at short distances. Reference [24] elaborated on this physical mechanism by elucidating how the two-body suppression leads to appearance of the universal barrier at  $R_3 \approx 2r_{\text{vdW}}$ .

As for the  $^4\text{He}$  trimer interacting with a realistic  $^4\text{He}$  potential that has a strong repulsive core at  $r \approx r_{\text{vdW}}$  and supports only one two-body bound state, one of the present authors (E.H.) and the collaborators [20] showed, by performing a nonadiabatic three-body calculation,  $a_-^{(0)}/r_{\text{vdW}} = 9.8$ , which is consistent with the observed value of the three-body parameter in alkali atoms.

One of the aims of the present paper is, using the same framework of our previous papers [26] and [27] (hereafter referred to as paper I and paper II, respectively), to calculate the Efimov spectra of the  $^4\text{He}$  trimer with the

\*Electronic address: hiyama@riken.jp

†Electronic address: mkamimura@riken.jp

seven different realistic  $^4\text{He}$  potentials [28–37]. We show that the calculated three-body parameters  $a_-^{(v)}/r_{\text{vdW}}$  for the ground ( $v = 0$ ) and excited ( $v = 1$ ) states are independent of the difference in the short-range details of the realistic potentials and are consistent with the observed values of the first and second Efimov resonances in the experiments for the alkali trimers.

From the  $^4\text{He}$  trimer wave functions described with the full three sets of the Jacobi coordinates, we derive the three-body potential  $U_3(R_3)$  as a function of the three-body hyperradius  $R_3$  and show that the potential has a repulsive core at  $R_3 \approx 2r_{\text{vdW}}$  and the three-body probability density inside the core is heavily suppressed both in the ground and excited states. This supports, from the view point of the realistic interactions, the finding [18, 24] of the appearance of the three-body repulsion universally at  $R_3 \approx 2r_{\text{vdW}}$  in the first Efimov trimer state.

As long as the tetramers of the alkali atoms are concerned, recent experiments have observed the scattering lengths  $a_-^{(4,0)}$  and  $a_-^{(4,1)}$ , at which the first and second universal four-body states tied to the first Efimov trimer state emerges at the four-body threshold on the  $a < 0$  side. The data [2, 7, 14, 15] exhibit a universal property  $a_-^{(4,0)}/r_{\text{vdW}} = -(3 \sim 4.5)$  and  $a_-^{(4,1)}/r_{\text{vdW}} = -(7 \sim 9)$ .

Another aim of this paper is to calculate the four-body Efimov spectra of the  $^4\text{He}$  tetramer states ( $v = 0, 1$ ) associated with the trimer ground state using the same realistic  $^4\text{He}$  potentials as above and present that the calculated values of the  $a_-^{(4,0)}/r_{\text{vdW}}$  and  $a_-^{(4,1)}/r_{\text{vdW}}$  are consistent with the observed values and are independent of the details of the potentials at short inter-particle separations. From the calculated tetramer wave function described with the full 18 sets of the Jacobi coordinates, we derive a four-body potential  $U_4(R_4)$  as a function of the four-body hyperradius  $R_4$  and show that the repulsive core is located at  $R_4 \approx 3r_{\text{vdW}}$  and the four-body probability density inside the core is heavily suppressed both in the ground and excited states.

The region suppressed by the three-(four-)body barrier in the  $^4\text{He}$  trimer (tetramer) is significantly larger than the region that is trivially excluded by the two-body repulsive core at  $r \approx r_{\text{vdW}}$ , which makes the critical scattering lengths insensitive to the short-range physics.

This paper is organized as follows: In Sec. II, we briefly explain the method and realistic  $^4\text{He}$  potentials used in this paper. In Sec. III, we calculate the Efimov spectrum of the  $^4\text{He}$  trimer and derive the three-body parameters  $a_-^{(v)}(v = 0, 1)$  which are compared with the corresponding observed values. The three-body hyperradial potentials  $U_3^{(v)}(R_3)$  is derived. In Sec. IV, we calculate the Efimov spectrum of the  $^4\text{He}$  tetramer and derive the critical scattering lengths  $a_-^{(4,v)}(v = 0, 1)$  which are compared with the observed values. The four-body hyperradial potential  $U_4^{(v)}(R_4)$  is derived. Summary is given in Sec. V.

## II. METHOD AND INTERACTIONS

### A. Gaussian expansion method for few bodies

In order to solve accurately the three- and four-body Schrödinger equations for the  $^4\text{He}$  trimer and tetramer, we use the Gaussian expansion method (GEM) for few-body systems [38–42] which was precisely explained in papers I and II. We employ the seven kinds of realistic  $^4\text{He}$ - $^4\text{He}$  potentials; names of the potentials are LM2M2 [28], TTY [29], HFD-B [30], HFD-B3-FC11 [31–33], SAPT96 [33–35], CCSAPT07 [36], and PCKLJS [37]. Among them the PCKLJS potential is currently the most sophisticated as explained in paper II, while the LM2M2 has been most popularly used in the literature.

The realistic  $^4\text{He}$  potentials has a strong short-range repulsive core (Fig. 1), which makes it technically challenging to solve the low-energy few-body problems accurately. As was demonstrated in papers I and II, however, our method is quite suitable for describing both the short-range correlations (without *a priori* assumption of any two-body correlation function) and the long-range asymptotic behavior of the  $^4\text{He}$  trimer and tetramer.

The wave function of the  $A$ -body  $^4\text{He}$ -atom system ( $A = 2 - 4$ ), say  $\Psi_A$ , is obtained by solving the Schrödinger equation in the fully nonadiabatic manner:

$$\left[ T + \sum_{1=i < j}^A \lambda V_2(r_{ij}) - E_A \right] \Psi_A = 0, \quad (2.1)$$

where  $T$  is the kinetic energy and  $V_2(r_{ij})$  is the realistic  $^4\text{He}$  potential as a function of the pair separation  $r_{ij}$  (see below for the factor  $\lambda$ ).  $\Psi_A$  has the total angular momentum  $J = 0$ . The mass parameter is fixed to  $\frac{\hbar^2}{m} = 12.11928 \text{ KÅ}^2$  [43] where  $m$  is mass of  $^4\text{He}$  atom.

The  $^4\text{He}$  tetramer wave function  $\Psi_4$  is calculated by expanding it in terms of the totally symmetrized  $L^2$ -integrable  $K$ -type and  $H$ -type four-body Gaussian basis functions of the full 18 sets of the Jacobi coordinates as was explained in paper I. The expansion coefficients and eigenenergy  $E_4$  are determined by diagonalizing the Hamiltonian in the large function space. The nonlinear parameters, such as the Gaussian ranges in geometric progressions, taken in the calculation were explicitly tabulated in paper I. Similar prescription is applied to the trimer (dimer) wave function  $\Psi_3(\Psi_2)$ .

For plotting the three-(four-)body Efimov spectrum of the  $^4\text{He}$  trimer (tetramer), we calculate the energies of the ground and excited states,  $E_3^{(0)}$  and  $E_3^{(1)}$  ( $E_4^{(0)}$  and  $E_4^{(1)}$ ), as functions of the scattering length  $a$  of the two-body interaction. Following the literature [20, 44–46], we mimic the experimental tunability of the interatomic interactions via Feshbach resonances by directly altering the strength  $\lambda$  of the realistic  $^4\text{He}$  potential in Eq. (2.1), which leads to the desired change of  $a$  (when  $\lambda = 1$ , the potential equals to the original one).

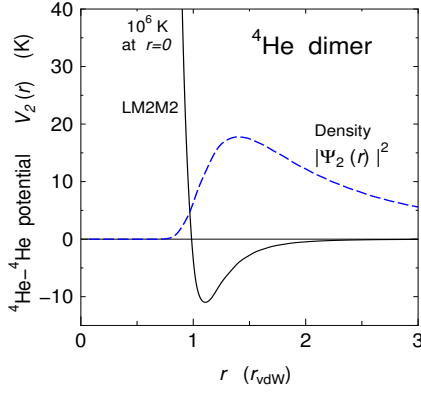


FIG. 1: The LM2M2 potential  $V_2(r)$ , one of the realistic  $^4\text{He}$  potentials, is shown as the black solid curve. The dashed blue curve shows the density of the dimer  $|\Psi_2(r)|^2$  (in arbitrary unit) at  $E_2 = -1.309$  mK, so weakly bound compared with the potential pocket of  $-11$  K.  $r_{\text{vdW}} = 5.08 a_0$ ,  $a_0$  being the Bohr radius.

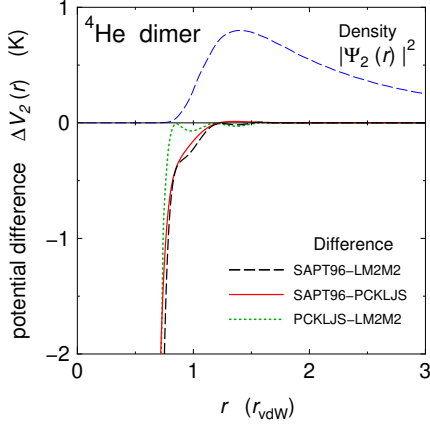


FIG. 2: Difference in the realistic  $^4\text{He}$  potentials  $V_2(r)$  between the three example potentials. The dimer energy is  $E_2 = -1.309$  mK (LM2M2),  $-1.615$  mK (PCKLJS) and  $-1.744$  mK (SAPT96). The repulsive core in the potentials is  $\approx 1000$  K at  $r = 0.7 r_{\text{vdW}}$ . The dashed blue curve is the same density of the dimer in Fig. 1 (in arbitrary unit).

The seven realistic  $^4\text{He}$  potentials have almost the same van der Waals potential  $-C_6/r^6$  but the binding energy of the  $^4\text{He}$  dimer ranges from 1.309 mK (LM2M2) to 1.744 mK (SAPT96) with some 30% difference (cf. Table I below) due to the variation in the short-range physics. We illustrate in Fig. 2 the potential differences between the three example potentials (LM2M2, PCKLJ and SAPT96). It is of interest to examine to what extent those differences affect the critical scattering lengths  $a_-^{(v)}$  in the  $^4\text{He}$  trimer and  $a_-^{(4,v)}$  in the tetramer.

## B. Three-(four-)body hyperradius

In order to investigate the short-range repulsive barrier in terms of the  $A$ -body hyperradius  $R_A$  ( $A = 3, 4$ ), we derive the hyperradial wave function from our wave function  $\Psi_A^{(v)}$ . Though there are several conventions to define  $R_A$ , the present paper employs the definition in Refs. [47, 48] for the  $A$ -body system with an equal mass:

$$R_A = \left[ \frac{2}{A} \sum_{j>i}^A (\mathbf{r}_i - \mathbf{r}_j)^2 \right]^{1/2}, \quad (2.2)$$

where  $\mathbf{r}_i$  is the position vector of particle  $i$ .

For the trimer, we have  $R_3 = \sqrt{\frac{2}{3}(r_{12}^2 + r_{13}^2 + r_{23}^2)}$  which was taken in the calculations in Refs. [1, 24, 46], while Ref. [18] employed another definition of  $R_3^{[18]} = \sqrt{\frac{1}{\sqrt{3}}(r_{12}^2 + r_{13}^2 + r_{23}^2)} \approx 0.93 R_3$ .

We define the probability density of the  $A$ -body system,  $\rho_A^{(v)}(R'_A)$  ( $A = 3, 4$  and  $v = 0, 1$ ), as a function of the hyperradius  $R'_A$  by

$$\rho_A^{(v)}(R'_A) = \langle \Psi_A^{(v)} | \frac{\delta(R_A - R'_A)}{R_A^{2D}} | \Psi_A^{(v)} \rangle, \quad (2.3)$$

where  $D$  is given by  $D = (3N - 1)/2$  with  $N = A - 1$  [47] and  $\rho_A^{(v)}(R_A)$  is normalized as  $\int_0^\infty \rho_A^{(v)}(R_A) R_A^{2D} dR = 1$  since  $\langle \Psi_A^{(v)} | \Psi_A^{(v)} \rangle = 1$ . In Appendix, we explain in more detail how we calculate Eq. (2.3) using  $\Psi_A^{(v)}$  which is written in terms of the full sets of Jacobi coordinates.

We relate the hyperradial density  $\rho_A^{(v)}(R_A)$  to the hyperradial wave function  $f_A^{(v)}(R_A)$  ( $v = 0, 1$ ) by

$$\rho_A^{(v)}(R_A) = \left| \frac{f_A^{(v)}(R_A)}{R_A^D} \right|^2, \quad (2.4)$$

and consider that  $f_A^{(v)}(R_A)$  satisfies the single-channel hyperradial Schrödinger equation for the  $^4\text{He}$  trimer and for the tetramer associated with the ground-state trimer:

$$\left[ -\frac{\hbar^2}{m} \frac{d^2}{dR_A^2} + U_A(R_A) - E_A^{(v)} \right] f_A^{(v)}(R_A) = 0, \quad (2.5)$$

(cf. Eq. (4.4) in Ref. [47], Eq. (6) in Ref. [24] and Eq. (1) in Ref. [18]) where the nonadiabatic effect and the coupling to other channels appearing in the hyperspherical framework are all renormalized into the  $A$ -body hyperradial potential  $U_A(R_A)$  since  $f_A^{(v)}(R_A)$  ( $v = 0, 1$ ) is calculated from the fully nonadiabatic solution  $\Psi_A^{(v)}$  and  $E_A^{(v)}$  of the original Schrödinger equation (2.1).

We derive  $U_A^{(v)}(R_A)$  ( $v = 0, 1$ ) by

$$U_A^{(v)}(R_A) = \frac{\hbar^2}{m} \frac{d^2 f_A^{(v)}(R_A)}{dR_A^2} / f_A^{(v)}(R_A) - E_A^{(v)}. \quad (2.6)$$

The result should satisfy  $U_A^{(0)}(R_A) = U_A^{(1)}(R_A)$  as the potential  $U_A(R_A)$  in the Schrödinger Eq. (2.5); this will successfully be examined in Secs. III B and IV B.

At large hyperradius, one would expect that  $U_3(R_3)$  asymptotes to

$$U_3(R_3) \rightarrow -\frac{\hbar^2}{m} \frac{s_0^2 + \frac{1}{4}}{R_3^2} \quad (R_3 \gg r_{\text{vdW}}) \quad (2.7)$$

with  $s_0 \approx 1.00624$  as the usual Efimov behavior of the potential [1, 18, 24]. It will be shown in Sec. IIIB that  $U_3^{(v)}(R_3)$  ( $v = 0, 1$ ) satisfy Eq. (2.7).

We note that if the two-body repulsive core at  $r_{12} \approx r_{\text{vdW}}$  is the direct origin of the repulsive barrier in  $U_A(R_A)$ , the particles could come close together reaching  $R_A \approx \sqrt{A-1} r_{\text{vdW}}$  when all the  $r_{ij} \approx r_{\text{vdW}}$  in Eq. (2.2); but this will be denied in Secs. IIIB and IVB since the possible minimum  $R_A$  is derived as  $R_A \approx (A-1) r_{\text{vdW}}$  ( $A = 3, 4$ ) in the actual calculation.

### III. RESULT FOR $^4\text{He}$ TRIMER

#### A. Three-body parameter

The calculated Efimov spectrum for the  $^4\text{He}$  trimer is plotted in Fig. 3 with the solid curves; the trimer energies  $E_3^{(0)}$  and  $E_3^{(1)}$  are illustrated as functions of the scattering length  $a$ . Following the literature, we have drawn  $(|E|/E_{\text{vdW}})^{1/4}$  versus  $(|a|/r_{\text{vdW}})^{-1/2}$  so that both curves are graphically represented on the same scale. The scattering length  $a$  and the energy  $E$  are scaled with  $r_{\text{vdW}}$  ( $= 5.08 a_0$ ) and the van der Waals energy  $E_{\text{vdW}} = \hbar^2/mr_{\text{vdW}}^2$  ( $= 1.677$  K), respectively. The dashed curve shows the dimer energy. The vertical dotted line indicates the physical value  $\lambda = 1$ .

The result in Fig. 3 depends little on the seven kinds of the realistic potentials so that the curves are the same for different potentials within the thickness of the lines. We note that, in the case of the LM2M2 potential, almost the same figure as Fig. 3 was already reported by one of the authors (E.H.) and the collaborators [20] and by Gottobigio *et al.* [46].

In Fig. 3,  $a_-^{(0)}$  and  $a_-^{(1)}$  indicate the critical scattering lengths at which the trimer energies  $E_3^{(0)}$  and  $E_3^{(1)}$  intersect respectively the three-atom threshold on the  $a > 0$  side. The calculated values of them are summarized in Table I together with the recent experimental values for the alkali-atom trimers [5–16]. First of all, we emphasize that the seven realistic potentials give the same value as  $a_-^{(0)}/r_{\text{vdW}} = -9.49(1)$  and  $a_-^{(1)}/r_{\text{vdW}} = -164(1)$  showing a negligible contribution from the difference in their short-range details shown in Fig. 2. The calculated value of  $a_-^{(0)}/r_{\text{vdW}}$  agrees with the universal value  $a_-^{(0)}/r_{\text{vdW}} \approx -9.5 \pm 15\%$  obtained in the recent experiments, while  $a_-^{(1)}/r_{\text{vdW}}$  for the excited state of the  $^4\text{He}$  trimer [56] is close to the observed values  $a_-^{(1)}/r_{\text{vdW}} = 177 \sim 200$  for the second Efimov resonances in  $^6\text{Li}$  and  $^{133}\text{Cs}$ .

The low-energy universal Efimov theory does not predict the absolute position of  $a_-^{(0)}$ , but predicts the

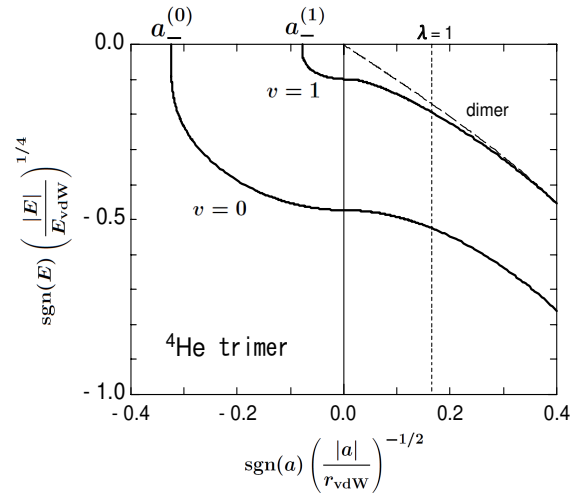


FIG. 3: Efimov spectrum for the  $^4\text{He}$  trimer calculated with the seven realistic  $^4\text{He}$  potentials, LM2M2, TTY, HFD-B, HFD-B3-FCI1, SAPT96, CCSAPT07, and PCKLJS: trimer energy  $E_3^{(v)}$  as a function of the scattering length  $a$  for the ground ( $v = 0$ ) and excited ( $v = 1$ ) states are shown as the solid curves, while the dimer energy is shown as the dotted curve. The curves for different potentials overlap with each other within the line thickness. To clarify the figure,  $a$  and  $E$  are scaled with the  $r_{\text{vdW}}$  and  $E_{\text{vdW}}$ , and raised to the power  $-1/2$  and  $1/4$ , respectively.  $a_-^{(0)}$  and  $a_-^{(1)}$  denote respectively the scattering lengths where the trimer energies  $E_3^{(0)}$  and  $E_3^{(1)}$  intersect the three-atom threshold. The dotted line indicates the scattering length corresponding to the unscaled potential at  $\lambda = 1$ .

ratio  $a_-^{(1)}/a_-^{(0)}$  to have a universal value  $a_-^{(1)}/a_-^{(0)} = 22.7$  [1, 3, 4]. According to the literature [23, 50–53], effects of the finite interaction range and the van der Waals tail give corrections toward somewhat smaller values than 22.7; especially, a value of 17.1 was predicted in Ref. [23] in the limit of strongly entrance-channel-dominated Feshbach resonances. The experiments that measured both the  $a_-^{(0)}$  and  $a_-^{(1)}$  in the same atom gave the ratio  $(a_-^{(1)}/a_-^{(0)})_{\text{exp}} = 21.0(1.3)$  and  $19.7$  for  $^{133}\text{Cs}$  [16] and  $^6\text{Li}$  [9, 10] respectively. With the present calculation of the  $^4\text{He}$  trimer using the realistic potentials, we have also found that the ratio gets smaller than the universal value, giving  $(a_-^{(1)}/a_-^{(0)})_{^4\text{He}} = 17.2$  [57].

#### B. Three-body repulsive barrier

Following the formulation of the hyperradial three-body potential in Sec. IIB, we first calculate the wave function  $\Psi_3^{(v)}$  in Eq. (2.1) using the LM2M2 potential, as an example (use of the other potentials give almost the same result), at the unitary limit ( $|a| \rightarrow \infty$ ) given by  $\lambda = 0.9743$ . We obtain  $E_3^{(0)} = -0.0501 E_{\text{vdW}}$  and  $E_3^{(1)} = -9.36 \times 10^{-5} E_{\text{vdW}}$ ; the r.m.s. radius  $\langle R_3^2 \rangle^{1/2}$  is  $6.47 r_{\text{vdW}}$  ( $v = 0$ ) and  $94.2 r_{\text{vdW}}$  ( $v = 1$ ).

TABLE I: Scattering lengths for the first and second Efimov resonances,  $a_-^{(0)}$  and  $a_-^{(1)}$ , where the Efimov spectra ( $v = 0, 1$ ) across the three-body threshold on the negative  $a$  side (cf. Fig. 3). They are calculated using the seven different realistic  $^4\text{He}$  potentials (see text for them and  $\lambda$ ) and compared with experimental values scaled with  $r_{\text{vdW}}$ . Here,  $r_{\text{vdW}}/a_0 = 5.08, 31.26, 32.49, 82.10$  and  $101$  for  $^4\text{He}$ ,  $^6\text{Li}$ ,  $^7\text{Li}$ ,  $^{85}\text{Rb}$  and  $^{133}\text{Cs}$ , respectively [49],  $a_0$  being the Bohr radius. The potential names are arranged in the increasing order of the binding energy of the  $^4\text{He}$  dimer,  $B_2$ , at  $\lambda = 1$ .

$^4\text{He}$ trimer		Ground state ( $v = 0$ )			Excited state ( $v = 1$ )		
Realistic potentials	$B_2$ (mK)	$a_-^{(0)}/a_0$	$a_-^{(0)}/r_{\text{vdW}}$	$\lambda$	$a_-^{(1)}/a_0$	$a_-^{(1)}/r_{\text{vdW}}$	$\lambda$
LM2M2	1.309	-48.26 <sup>a</sup>	-9.50	0.8901	-832 <sup>a</sup>	-164	0.9685
TTY	1.316	-48.29	-9.50	0.8902	-832	-164	0.9685
HFD-B3-FCI1	1.448	-48.22	-9.49	0.8891	-832	-164	0.9673
CCSAPT07	1.564	-48.21	-9.49	0.8881	-832	-164	0.9662
PCKLJS	1.615	-48.21	-9.49	0.8877	-832	-164	0.9658
HFD-B	1.692	-48.22	-9.49	0.8869	-832	-164	0.9651
SAPT96	1.744	-48.18	-9.48	0.8867	-831	-164	0.9647
Exp( $^{133}\text{Cs}$ , $^{85}\text{Rb}$ , $^6,^7\text{Li}$ )		$\approx -9.5 \pm 15\%$ <sup>b</sup>					
Exp ( $^{133}\text{Cs}$ ) [16]		-963(11)	-9.53(11)		-20190(1200)	-200(12)	
Exp ( $^6\text{Li}$ ) [9, 10]		-292	-9.34		-5752	-177	

<sup>a</sup>Ref. [46] gave  $a_-^{(0)}/a_0 = -48.1$  and  $a_-^{(1)}/a_0 = -975$  for LM2M2.

<sup>b</sup>A value summarized in [12, 17–19] for experimental data [5–16].

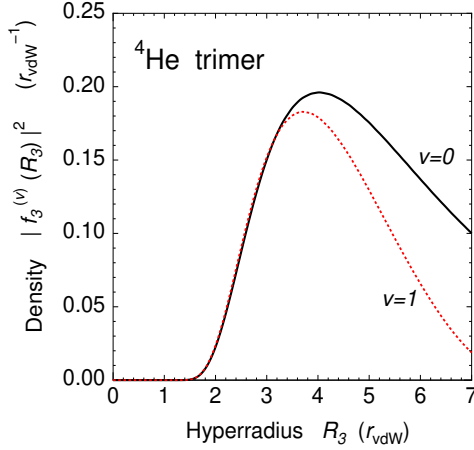


FIG. 4: Probability density  $|f_3^{(v)}(R_3)|^2$  ( $v = 0, 1$ ) of the  $^4\text{He}$  trimer ground (solid curve) and excited (dotted red curve) states versus the three-body hyperradius  $R_3$  for  $R_3 < 7 r_{\text{vdW}}$ . The dotted curve has been multiplied by a factor 463 to emphasize that the two states exhibit the same shape of the strong short-range correlations for  $R_3 \lesssim 3 r_{\text{vdW}}$ .

Calculated three-body densities  $|f_3^{(v)}(R_3)|^2$  are illustrated in Fig. 4 for  $R_3 < 7 r_{\text{vdW}}$  and in Fig. 5 (log scale) for  $R_3 < 25 r_{\text{vdW}}$  as the solid curve ( $v = 0$ ) and the dotted red curve ( $v = 1$ ). In Fig. 6, the three-body potentials  $U_3^{(v)}(R_3)$  defined by Eq. (2.6) are shown as the solid curve ( $v = 0$ ) and the dotted red curve ( $v = 1$ ). Also shown, for the sake of reference, are the Efimov at-

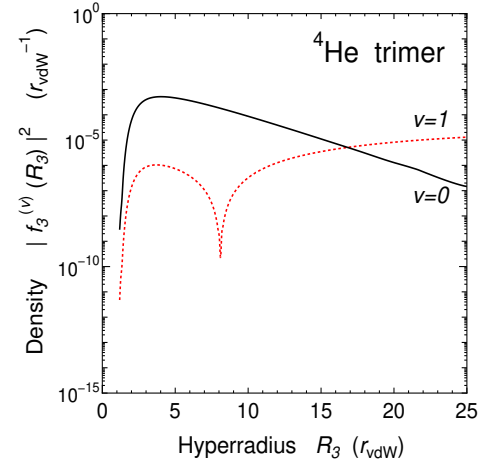


FIG. 5: The same as Fig. 4 for  $R_3 < 25 r_{\text{vdW}}$  in the log sale, but no factor is multiplied to the dotted curve.

traction, Eq. (2.7), in the dot-dash curve and the density  $|f_3^{(0)}(R_3)|^2$  in the dashed blue curve (arbitrary unit).

A striking aspect of these figures is that the hyperradial potentials satisfy  $U_3^{(0)}(R_3) = U_3^{(1)}(R_3)$  and converge to the Efimov attraction at large distances; this demonstrates the validity of the idea to construct the hyperradial Schrödinger equation (2.5) starting from the solution  $\Psi_3^{(v)}$  and  $E_3^{(v)}$  of the original Schrödinger equation (2.1).

From the behavior of the potentials  $U_3^{(v)}(R_3)$  and the

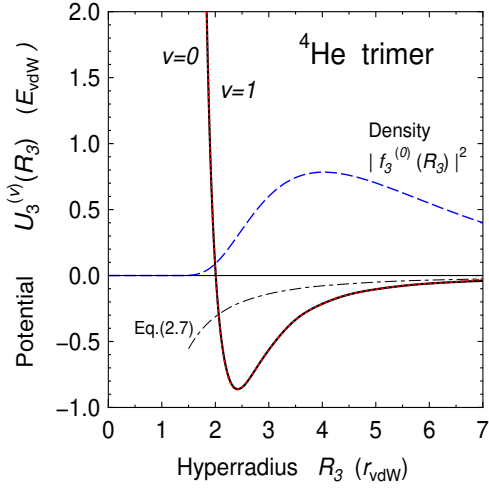


FIG. 6: The three-body potential  $U_3^{(v)}(R_3)$  ( $v = 0, 1$ ) defined by Eq. (2.6) for the trimer ground (solid curve) and excited (dotted red curve) states. The two curves overlap with each other within the thickness of the lines. The dash-dotted curve shows the Efimov attraction, Eq. (2.7), and the dashed blue curve is for the density  $|f_3^{(0)}(R_3)|^2$  in arbitrary unit.

densities  $|f_3^{(v)}(R_3)|^2$  ( $v = 0, 1$ ), we recognize that there is a three-body repulsive barrier at  $R_3 \approx 2r_{vdW}$ . Inside the barrier,  $R_3 \lesssim 2r_{vdW}$ , the probability of finding the atoms is heavily suppressed. This result supports the finding, in Refs.[18, 24], of the appearance of the effective three-body repulsion with the adiabatic hyperspherical calculations. Our potential in Fig. 6 is close to the the hyperradial three-body potential for the first Efimov trimer state obtained in Fig. 3b of Ref. [18] and Figs. 1 and 7 of Ref. [24].

The hyperradius  $R_3 \approx 2r_{vdW}$  of the three-body repulsive barrier corresponds to the inter-particle distance  $r_{ij} \approx \sqrt{2}r_{vdW}$  when all the  $r_{ij}$  are equal to each other in Eq. (2.2). The distance is  $\sqrt{2}$  times larger than the radius of the two-body potential core  $r_{12} \approx r_{vdW}$  and is located almost outside the region where the difference in the seven realistic potentials is seen in Fig. 2; this is due to the nonadiabatic three-body dynamics that, as was pointed out in Refs. [18, 24], the suppression of the two-body probability for  $r_{ij} \lesssim r_{vdW}$  leads to the three-body repulsion for  $R_3 \lesssim 2r_{vdW}$ .

#### IV. RESULT FOR $^4\text{He}$ TETRAMER

##### A. Four-body Efimov spectrum

Using the same method of papers I and II, we solved the four-body Schrödinger equation (2.1) for the ground ( $v = 0$ ) and excited ( $v = 1$ ) states of the  $^4\text{He}$  tetramer changing the factor  $\lambda$  for the potentials. The four-body Efimov spectrum of  $E_4^{(0)}$  and  $E_4^{(1)}$  is plotted in Fig. 7 in

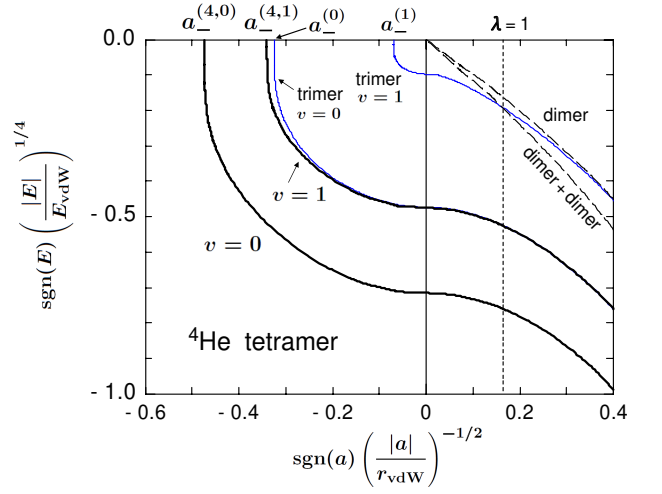


FIG. 7: Efimov spectrum for the  $^4\text{He}$  tetramer calculated with the seven realistic  $^4\text{He}$  potentials, LM2M2, TTY, HFD-B, HFD-B3-FCI1, SAPT96, CCSAPT07, and PCKLJS: The scaled tetramer energy  $E_4^{(v)}/E_{vdW}$  as a function of the scaled inverse scattering length  $(a/r_{vdW})^{-1}$  for the ground ( $v = 0$ ) and excited ( $v = 1$ ) states. The curves for different potentials overlap with each other within the line thickness. The thin solid blue curves denote the trimer spectrum which is the same as that in Fig. 3.  $a_-^{(4,0)}$  and  $a_-^{(4,1)}$  denote the critical scattering lengths where the tetramer energies  $E_4^{(0)}$  and  $E_4^{(1)}$  cross the four-atom threshold, respectively.

the solid curves together with the spectrum of  $^4\text{He}$  trimer in the thin solid blue curves.

We note that the four-body Efimov plot for the  $^4\text{He}$  tetramer calculated with the *realistic*  $^4\text{He}$  potential is reported for the first time in the present paper. Using effective two-body plus three-body Gaussian potentials, Gattobigio *et. al* [46] obtained a similar plot as Fig. 7 for the  $^4\text{He}$  tetramer. We find two tetramer bound states, one deep and one shallow, tied to the trimer ground state; this agrees with the key prediction in Refs. [54, 55] that there are two universal four-body states associated with each Efimov trimer.

In Fig. 7,  $a_-^{(4,0)}$  and  $a_-^{(4,1)}$  denote the critical scattering lengths where the tetramer energies  $E_4^{(0)}$  and  $E_4^{(1)}$  cross the four-atom threshold. Their values are summarized in Table II for the realistic  $^4\text{He}$  potentials together with the observed values for  $^{133}\text{Cs}$  [2, 7, 15] and  $^7\text{Li}$  [14]. Similarly to Table I for the trimer, the seven realistic potentials give the same value as  $a_-^{(4,0)}/r_{vdW} = -4.46(1)$  and  $a_-^{(4,1)}/r_{vdW} = -8.65(1)$  showing that they are insensitive to the details of the potentials at short distances [58]. The calculated values are consistent with the observed values for the  $^{133}\text{Cs}$  and  $^7\text{Li}$  tetramers as seen in Table II.

Reference [55] predicted that the universal properties of the four-body system are directly related to the three-body subsystem as  $a_-^{(4,0)} = 0.43 a_-^{(0)}$  and



TABLE II: The critical scattering lengths  $a_-^{(4,0)}$  and  $a_-^{(4,1)}$ , where the tetramer energies  $E_4^{(0)}$  and  $E_4^{(1)}$  cross the four-body threshold on the negative  $a$  side (see Fig. 7). They are calculated with the seven different realistic  $^4\text{He}$  potentials (see text for them and  $\lambda$ ) and are compared with experimental values for alkali atoms.  $B_2$  is the binding energy of the dimer at  $\lambda = 1$ .

$^4\text{He}$ tetramer		Ground state ( $v = 0$ )			Excited state ( $v = 1$ )		
Realistic potentials	$B_2$ (mK)	$a_-^{(4,0)}/a_0$	$a_-^{(4,0)}/r_{\text{vdW}}$	$\lambda$	$a_-^{(4,1)}/a_0$	$a_-^{(4,1)}/r_{\text{vdW}}$	$\lambda$
LM2M2	1.309	-22.69	-4.47	0.8197	-43.98	-8.66	0.8832
TTY	1.316	-22.70	-4.47	0.8199	-43.96	-8.65	0.8832
HFD-B3-FCI1	1.448	-22.67	-4.46	0.8187	-43.95	-8.65	0.8821
CCSAPT07	1.564	-22.66	-4.46	0.8178	-43.95	-8.65	0.8812
PCKLJS	1.615	-22.66	-4.46	0.8174	-43.93	-8.65	0.8807
HFD-B	1.692	-22.67	-4.46	0.8166	-43.95	-8.65	0.8800
SAPT96	1.744	-22.65	-4.46	0.8165	-43.91	-8.64	0.8798
Exp ( $^{133}\text{Cs}$ ) [2]		-444(8)	-4.40(8)		-862(9)	-8.53(9)	
Exp ( $^{133}\text{Cs}$ ) [7]		-410	-4.06		-730	-7.23	
Exp ( $^{133}\text{Cs}$ ) [15]		-440(10)	-4.36(10)				
Exp ( $^7\text{Li}$ ) [14]		-94(4)	-2.9(1)		-236(10)	-7.26(31)	

$a_-^{(4,1)} = 0.90 a_-^{(0)}$ . The present calculation of the  $^4\text{He}$  atoms using the realistic potentials gives consistent values of  $a_-^{(4,0)} = 0.47 a_-^{(0)}$  and  $a_-^{(4,1)} = 0.91 a_-^{(0)}$ . The observed data for  $^{133}\text{Cs}$  and  $^7\text{Li}$  are in accordance with the prediction [55].

### B. Four-body repulsive barrier

Using the nonadiabatic solution  $\Psi_4^{(v)}$  ( $v = 0, 1$ ) to the four-body Schrödinger equation (2.1), we calculate the probability density  $|f_4^{(v)}(R_4)|^2$  and the potential  $U_4^{(v)}(R_4)$ , defined in Sec. II, as functions of the four-body hyperradius  $R_4 = \sqrt{\frac{1}{2}(r_{12}^2 + r_{13}^2 + r_{14}^2 + r_{23}^2 + r_{24}^2 + r_{34}^2)}$ . As for the  $^4\text{He}$  realistic potential, we employ, the LM2M2 potential, as an example (use of the other potentials give almost the same result), at the unitary limit ( $|a| \rightarrow \infty$ ) with  $\lambda = 0.9743$ ; we have  $E_4^{(0)} = -0.262 E_{\text{vdW}}$  and  $E_4^{(1)} = -0.0510 E_{\text{vdW}}$ . The r.m.s. hyperradius  $\langle R_4^2 \rangle^{1/2}$  is  $5.95 r_{\text{vdW}}$  ( $v = 0$ ) and  $38.0 r_{\text{vdW}}$  ( $v = 1$ ).

The density distributions  $|f_4^{(v)}(R_4)|^2$  are illustrated in Fig. 8 for  $R_4 < 10 r_{\text{vdW}}$  and in Fig. 9 (log scale) for  $R_4 < 25 r_{\text{vdW}}$  by the solid curve ( $v = 0$ ) and the dotted red curve ( $v = 1$ ). The four-body potentials  $U_4^{(v)}(R_4)$  are shown in Fig. 10 as the solid curve ( $v = 0$ ) and the dotted red curve ( $v = 1$ ) [59].

We find that the condition  $U_4^{(0)}(R_4) = U_4^{(1)}(R_4)$  is satisfied, which demonstrates the validity of the picture based on the hyperradial Schrödinger equation (2.5) for the tetramer states attached to the trimer ground state. From the behavior of the potentials  $U_4^{(v)}(R_4)$  and the density distributions  $|f_4^{(v)}(R_4)|^2$  ( $v = 0, 1$ ), we recognize a

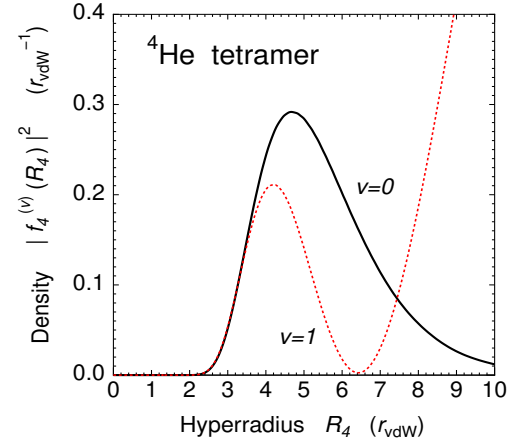


FIG. 8: Probability density  $|f_4^{(v)}(R_4)|^2$  ( $v = 0, 1$ ) of the  $^4\text{He}$  tetramer ground (solid curve) and excited (dotted red curve) states as a function of the hyperradius  $R_4$  for  $R_4 < 10 r_{\text{vdW}}$ . The density is normalized as  $\int_0^\infty |f_4^{(v)}(R_4)|^2 dR_4 = 1$ . The dotted curve has been multiplied by a factor 25 to emphasize that the two tetramer states exhibit the same shape of the strong short-range correlations for  $R_4 \lesssim 3.5 r_{\text{vdW}}$ .

strong repulsive barrier at  $R_4 \approx 3 r_{\text{vdW}}$  that heavily suppresses the four-body density in the region  $R_4 \lesssim 3 r_{\text{vdW}}$ , which makes  $a_-^{(4,0)}$  and  $a_-^{(4,1)}$  insensitive to the short-range details of the interactions seen in Fig. 2.

The four-body repulsion radius  $R_4 \approx 3 r_{\text{vdW}}$  corresponds to the interparticle distance  $r_{ij} \approx \sqrt{3} r_{\text{vdW}}$  when all the  $r_{ij}$  are equal to each other in Eq. (2.2). The distance is  $\sqrt{3}$  times larger than the two-body core radius  $r_{12} \approx r_{\text{vdW}}$  and is located outside the region where

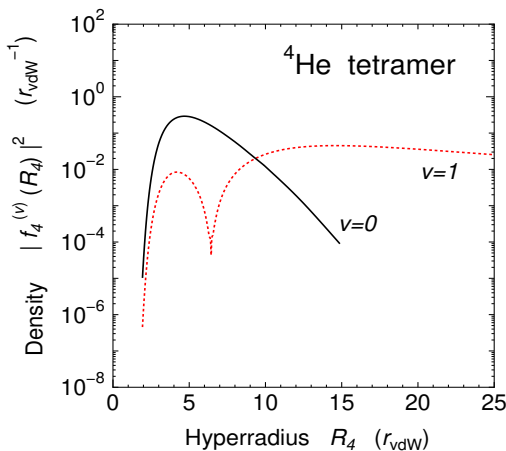


FIG. 9: The same as Fig. 8 for  $R_4 < 25 r_{\text{vdW}}$  in the log scale, but no factor is multiplied to the dotted curve.

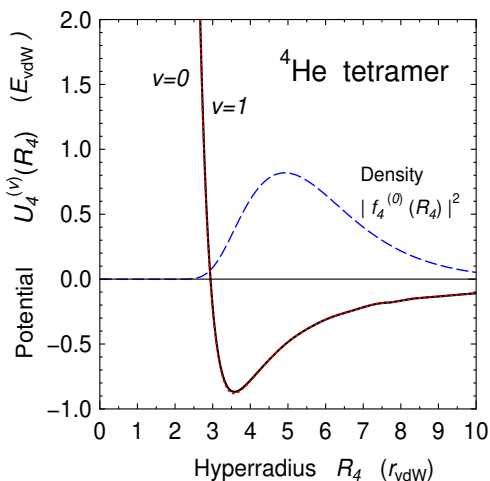


FIG. 10: The four-body potential  $U_4^{(v)}(R_4)$  ( $v = 0, 1$ ) defined by Eq. (2.6) for the  $^4\text{He}$  tetramer ground (solid curve) and excited (dotted red curve) states. The two curves overlap with each other within the thickness of the lines. The dashed blue curve is for the density  $|f_4^{(0)}(R_4)|^2$  in arbitrary unit.

the short-range details of the seven realistic potentials differ from each other (Fig. 2). Inversely, if all the  $r_{ij}$  are artificially replaced by the two-body core radius, the four-body repulsion radius becomes  $R_4 \approx \sqrt{3} r_{\text{vdW}}$ . The increase of the core radius  $R_4$  by factor  $\sqrt{3}$  in the actual four-body system is due to the nonadiabatic four-body dynamics which is an extension of the mechanism discovered in Ref. [18] for the three-body systems.

It will be one of the future subjects whether the four-body repulsive barrier at hyperradius  $R_4 \approx 3 r_{\text{vdW}}$  also appears for deeper pairwise interactions that supports many two-body bound states like alkali atoms.

## V. SUMMARY

We have investigated the universality in the  $^4\text{He}$  trimer and tetramer using the seven realistic  $^4\text{He}$ - $^4\text{He}$  potentials. We calculated the critical scattering lengths  $a_-^{(v)}$  ( $a_-^{(4,v)}$ ) ( $v = 0, 1$ ) at which the trimer (tetramer) energies cross the three-(four-)atom threshold. From the nonadiabatic total wave function  $\Psi_A^{(v)}(A = 3, 4)$  that is described in terms of the full sets of the Jacobi coordinates, we derived the hyperradial wave function  $f_A^{(v)}(R_A)$  and potential  $U_A^{(v)}(R_A)$  as a function of the  $A$ -body hyperradius  $R_A$ . The main conclusions are summarized as follows:

(i) We found the following universality in the  $^4\text{He}$  tetramer: The four-body hyperradial potentials  $U_4^{(v)}(R_4)$  ( $v = 0, 1$ ) have a repulsive barrier at the four-body hyperradius  $R_4 \approx 3 r_{\text{vdW}}$ , which corresponds to the pair distance  $r_{ij} \approx \sqrt{3} r_{\text{vdW}}$  when all the  $r_{ij}$  are equal to each other. This pair distance is significantly larger than the radius  $r_{12} \approx r_{\text{vdW}}$  of the two-body repulsive core in the realistic  $^4\text{He}$  potentials. Inside the barrier,  $R_4 \lesssim 3 r_{\text{vdW}}$ , the probability density  $|f_4^{(v)}(R_4)|^2$  to find the atoms is heavily suppressed. The four-body barrier prevents the particles from getting close together to explore non-universal features of the interactions at short distances; hence, the critical scattering lengths are not affected by the difference in the short-range details of the interactions. The seven realistic  $^4\text{He}$  potentials give the same value as  $a_-^{(4,0)}/r_{\text{vdW}} = -4.46(1)$  and  $a_-^{(4,1)}/r_{\text{vdW}} = -8.65(1)$ , which are consistent with the corresponding values obtained in the experiments in ultracold gases of the alkali-metal atoms.

(ii) As for the universality in the  $^4\text{He}$  trimer, we obtained the following result, which is consistent with that has been reported in Refs. [18, 24]: The three-body hyperradial potentials  $U_3^{(v)}(R_3)$  ( $v = 0, 1$ ) have a repulsive barrier at  $R_3 \approx 2 r_{\text{vdW}}$ , inside which the probability density  $|f_3^{(v)}(R_3)|^2$  of finding the atoms is heavily suppressed. The hyperradius of the barrier corresponds to the pair distance  $r_{ij} \approx \sqrt{2} r_{\text{vdW}}$  when all the  $r_{ij}$  are equal to each other. The seven realistic  $^4\text{He}$  potentials give the same value of the universal three-body parameters as  $a_-^{(0)}/r_{\text{vdW}} = -9.49(1)$  and  $a_-^{(1)}/r_{\text{vdW}} = -164(1)$  independently of the short-range details of the potentials and are consistent with the corresponding values obtained in the ultracold-atom experiments.

(iii) For four-body bound states, the universal repulsion appears at larger distance than the three-body ones, suggesting that the four-body states tend to be more universal than the three-body ones. As a natural extension, we conjecture that the universal  $N$ -body repulsive barrier ( $N > 4$ ) would generally appear in the Efimov associated  $N$ -body bound states, rendering the  $N$ -body states insensitive to short-range details and universal.



## Appendix

We explain how to calculate the density  $\rho_3(R)$  of Eq. (2.3) (the suffix 3 of  $R_3$  is omitted). It is difficult to perform the integration (2.3) with the hyperradius  $R$  treated explicitly since  $\Psi_3$  is not given as a function of  $R$ . We expand  $\rho_3(R)$  in terms of Gaussians

$$\rho_3(R) = \sum_{n=1}^{n_{\max}} c_n e^{-\nu_n R^2} \quad (5.1)$$

taking the range parameters  $\{\nu_n\}$  in a geometric progression (e.g. Eqs. (2.10)–(2.13) in paper I). The coefficients  $c_n$  are obtained by solving a set of linear equations

$$\sum_{n=1}^{n_{\max}} A_{in} c_n = B_i \quad (i = 1, \dots, n_{\max}) \quad (5.2)$$

with the matrix elements

$$A_{in} = \int_0^\infty e^{-(\nu_i + \nu_n)R^2} R^5 dR = (\nu_i + \nu_n)^{-3}, \quad (5.3)$$

$$\begin{aligned} B_i &= \int_0^\infty \rho_3(R') e^{-\nu_i R'^2} R'^5 dR' = \langle \Psi_3 | e^{-\nu_i R^2} | \Psi_3 \rangle \\ &= \langle \Psi_3 | e^{-\frac{2}{3}\nu_i(r_{12}^2 + r_{23}^2 + r_{31}^2)} | \Psi_3 \rangle. \end{aligned} \quad (5.4)$$

$B_i$  is nothing but the expectation value of a three-body force of Gaussian shape, which is easily calculated. We took the set of Gaussian ranges in a geometric progression  $\{n_{\max} = 60, R_1 = 0.2 r_{\text{vdW}}, R_{\max} = 80 r_{\text{vdW}}\}$  where  $\nu_n = 1/R_n^2$ .

We also apply this method to the case of  $^4\text{He}$  tetramer.

## Acknowledgement

The authors would like to thank Dr. S. Endo for valuable discussions and careful reading the manuscript. The numerical calculations were performed on HITACHI SR16000 at KEK and at YIFP in Kyoto University.

- 
- [1] V. Efimov, *Yad. Fiz.* **12**, 1080 (1970) [*Sov. J. Nucl. Phys.* **12**, 589 (1971)]; *Nucl. Phys. A* **210**, 157 (1973).
  - [2] F. Ferlaino, A. Zenesini, M. Berninger, B. Huang, H.-C. Nägerl, and R. Grimm, *Few-Body Syst.* **51**, 113 (2011)
  - [3] E. Braaten and H-W. Hammer, *Phys. Reports*, **428**, 259 (2006).
  - [4] E. Braaten and H-W. Hammer, *Annals of Physics* **322**, 120 (2007).
  - [5] T. Kraemer, M. Mark, P. Waldburger, J.G. Danzl, C. Chin, B. Engeser, A.D. Lange, K. Pilch, A. Jaakkola, H.-C. Nägerl, R. Grimm, *Nature* **440**, 315 (2006).
  - [6] S.E. Pollack, D. Dries, and R.G. Hulet, *Science* **326**, 1683 (2009).
  - [7] F. Ferlaino, S. Knoop, M. Berninger, W. Harm, J.P.D Incao, H.-C. Nägerl, and R. Grimm, *Phys. Rev. Lett.* **102**, 140401 (2009).
  - [8] N. Gross, Z. Shotan, S. Kokkelmans, and L. Khaykovich, *Phys. Rev. Lett.* **103**, 163202 (2009).
  - [9] A.N. Wenz, T. Lompe, T.B. Ottenstein, F. Serwane, G. Zürn, and S. Jochim, *Phys. Rev. A* **80**, 040702(R) (2009).
  - [10] J.R. Williams, E.L. Hazlett, J.H. Huckans, R.W. Stites, Y. Zhang, and K.M. O'Hara, *Phys. Rev. Lett.* **103**, 130404 (2009).
  - [11] N. Gross, Z. Shotan, S. Kokkelmans, and L. Khaykovich, *Phys. Rev. Lett.* **105**, 103203 (2010).
  - [12] M. Berninger, A. Zenesini, B. Huang, W. Harm, H.-C. Nägerl, F. Ferlaino, R. Grimm, P. S. Julienne, and J.M. Hutson, *Phys. Rev. Lett.* **107**, 120401 (2011).
  - [13] R. Wild, P. Makotyn, P.M. Pino, E.A. Cornell, and D.S. Jin, *Phys. Rev. Lett.* **108**, 145305 (2012).
  - [14] P. Dyke, S.E. Pollack, and G. Hulet, *Phys. Rev. A* **88**, 023625 (2013).
  - [15] A. Zenesini, B. Huang, M. Berninger, S. Besler, H.-C. Nägerl, F. Ferlaino, R. Grimm, C. H. Greene, and J. von Stecher, *New J. Phys.* **15**, 043040 (2013).
  - [16] B. Huang, L.A. Sidorenkov, R. Grimm, and J.M. Hutson, *Phys. Rev. Lett.* **112**, 190401 (2014).
  - [17] O. Machtey, Z. Shotan, N. Gross, and L. Khaykovich, *Phys. Rev. Lett.* **108**, 210406 (2012).
  - [18] J. Wang, J.P. D'Incao, B.D. Esry, and C.H. Greene, *Phys. Rev. Lett.* **108**, 263001 (2012).
  - [19] S. Roy, M. Landini, A. Trenkwalder, G. Semeghini, G. Spagnolli, A. Simoni, M. Fattori, M. Inguscio, and G. Modugno, *Phys. Rev. Lett.* **111**, 053202 (2013).
  - [20] P. Naidon, E. Hiyama and M. Ueda, *Phys. Rev. A* **86**, 012502 (2012).
  - [21] C. Chin, arXiv:1111.1484.
  - [22] P. K. Sørensen, D. V. Fedorov, A.S. Jensen, and N. T. Zinner, *Phys. Rev. A* **86**, 052516 (2012).
  - [23] R. Schmidt, S.P. Rath, and W. Zwerger, *Eur. Phys. J. B* **85**, 386 (2012).
  - [24] P. Naidon, S. Endo and M. Ueda, *Phys. Rev. A* **90**, 022106 (2014).
  - [25] P. Naidon, S. Endo and M. Ueda, *Phys. Rev. Lett.* **112**, 105301 (2014).
  - [26] E. Hiyama and M. Kamimura, *Phys. Rev. A* **85**, 022502 (2012).
  - [27] E. Hiyama and M. Kamimura, *Phys. Rev. A* **85**, 062505 (2012).
  - [28] R.A. Aziz and M.J. Slaman, *J. Chem. Phys.* **94**, 8047 (1991).
  - [29] K.T. Tang, J.P. Toennies and C.L. Yiu, *Phys. Rev. Lett.* **74**, 1546 (1995).
  - [30] R.A. Aziz, F.R.W. McCourt and C.C.K. Wong, *Mol. Chem. Phys.* **61**, 1487 (1987).
  - [31] T. van Mourik and J. H. van Lenthe, *J. Chem. Phys.* **102**, 7479 (1995).
  - [32] R. A. Aziz, A. R. Janzen, and M. R. Moldover, *Phys. Rev. Lett.* **74**, 1586 (1995).
  - [33] A.R. Jansen and R.A. Aziz, *J. Chem. Phys.* **107**, 914 (1997).
  - [34] H. L. Williams, T. Korona, R. Bukowski, B. Jeziorski, and K. Szalewicz, *Chem. Phys. Lett.* **262**, 431 (1996).
  - [35] T. Korona, H. L. Williams, R. Bukowski, B. Jeziorski, and K. Szalewicz, *J. Chem. Phys.* **106**, 5109 (1997).
  - [36] M. Jeziorska, W. Cencek, K. Patkowski, B. Jeziorski, and

- K. Szalewicz, J. Chem. Phys. **127**, 124303 (2007).
- [37] M. Przybytek, W. Cencek, J. Komasa, G. Lach, B. Jeziorski and K. Szalewicz, Phys. Rev. Lett. **104**, 183003 (2010); [Erratum], Phys. Rev. Lett. **108**, 129902.
- [38] M. Kamimura, Phys. Rev. A **38**, 621 (1988).
- [39] H. Kameyama, M. Kamimura and Y. Fukushima, Phys. Rev. C **40**, 974 (1989).
- [40] E. Hiyama, Y. Kino and M. Kamimura, Prog. Part. Nucl. Phys. **51**, 223 (2003).
- [41] E. Hiyama, Few-Body Systems **53**, 189 (2012).
- [42] E. Hiyama, Prog. Theor. Exp. Phys. **2012**, 01A204 (2012).
- [43] V. Roudnev and M. Cavagnero, J. Phys. B: At. Mol. Opt. Phys. **45**, 025101 (2012).
- [44] B.D. Esry, C.D. Lin, and C.H. Greene, Phys. Rev. A **54**, 394 (1996).
- [45] P. Barletta and A. Kievsky, Phys. Rev. A **64**, 042514 (2001).
- [46] M. Gattobigio, A. Kievsky, and M. Viviani, Phys. Rev. A **86**, 042513 (2012).
- [47] M. Fabre de la Ripplé, Ann. Phys.(N.Y.) **147**, 281 (1983).
- [48] M. Gattobigio, A. Kievsky, M. Viviani, and P. Barletta, Phys. Rev. A **79**, 032513 (2009).
- [49] C. Chin, R. Grimm, P.S. Julienne, and E. Tiesinga, Rev. Mod. Phys. **82**, 1225 (2010).
- [50] J.P. D’Incao, C. H. Greene, and B. D. Esry, J. Phys. B **42**, 044016 (2009).
- [51] L. Platter, C. Ji, and D.R. Phillips, Phys. Rev. A **79**, 022702 (2009).
- [52] M. Thøgersen, D.V. Fedorov, and A.S. Jensen, Phys. Rev. A **78**, 020501(R) (2008).
- [53] Y. Wang and P.S. Julienne, arXiv:1404.0483.
- [54] H.-W. Hammer and L. Platter, Eur. Phys. J. A **32**, 113 (2007).
- [55] J. von Stecher, J.P. D’Incao and C.H. Greene, Nature Phys., **5**, 417 (2009).
- [56] It is rather difficult to calculate precisely  $a_-^{(1)}$  of the excited trimer state that has an extremely large size at  $E_3^{(1)} \approx 0$ . We took the maximum range of the Gaussians to be  $4,000 r_{\text{vdW}}$  with the number of basis increased when calculating  $a_-^{(v)}(a_-^{(4,v)})$ . We note that, if a smaller-size (worse) three-body basis set is *artificially* employed, the solid curve ( $v = 1$ ) in Fig. 3 shifts slightly to the right (namely, the eigenstate becomes shallower), which gives a larger value of  $|a_-^{(1)}|/r_{\text{vdW}}$ , even *closer* to the corresponding observed data for the alkali atoms.
- [57] The same as the comments on  $|a_-^{(1)}|/r_{\text{vdW}}$  in [56] for the ratio  $a_-^{(1)}/a_-^{(0)}$ .
- [58] Using effective two-body plus three-body Gaussian potentials, Ref. [46] gave  $a_-^{(4,0)} = -19.6 a_0$  and  $a_-^{(4,1)} = -39.8 a_0$ , which correspond to  $a_-^{(4,0)}/r_{\text{vdW}} = -3.86$  and  $a_-^{(4,1)}/r_{\text{vdW}} = -7.83$ , respectively.
- [59] Since the dotted curve becomes singular in the vicinity of  $R_4 = 6.4 r_{\text{vdW}}$  where  $f_4^{(1)}(R_4) = 0$  in Eq. (2.6), we connected smoothly the lines on the both sides of the vicinity. When the Schrödinger equation (2.5) is solved using the smoothed potential, the condition that the excited-state wave function should have a node at  $R_4 = 6.4 r_{\text{vdW}}$  is guaranteed by the orthogonality to the ground-state wave function. This situation is the same for the case of the trimer excited state whose wave function  $f_3^{(1)}(R_3)$  has a node at  $R_3 = 8.1 r_{\text{vdW}}$  (Fig. 5).